Electronic supplementary information (ESI)

Pit-embellished low-valent metal active sites customize CO_2 photoreduction to methanol

Wei Zhao,[a] Miao Ding,[c] Pengxin Yang,[a] Qiang Wang,[a] Kaifu Zhang,*[a] Xiaowen Zhan,[e] Yu Yu,[a] Qiquan Luo,*[c] Shan Gao,*[a] Jinlong Yang[d] and Yi Xie*[b]

[a] *Anhui Province Key Laboratory of Chemistry for Inorganic/Organic Hybrid Functionalized Materials, Key Laboratory of Structure and Functional Regulation of Hybrid Materials of Ministry of Education, School of Chemistry and Chemical Engineering, Anhui University, Hefei, 230039, China. E-mail: shangao@ahu.edu.cn; kfzhang@ahu.edu.cn*

[b] *Hefei National Research Center for Physical Sciences at Microscale, University of Science & Technology of China, Hefei, 230026, China. E-mail: yxie@ustc.edu.cn*

[c] *Institutes of Physical Science and Information Technology, Anhui University, Hefei, 230039, China. E-mail: qluo@ustc.edu.cn*

[d] *Hefei National Research Center for Physical Sciences at Microscale, Synergetic Innovation Centre of Quantum Information & Quantum Physics, University of Science & Technology of China, Hefei, 230026, China.*

[e] *School of Materials Science and Engineering, Anhui University, Hefei, 230039, China.*

Methods

Chemicals

Sodium tungstate dihydrate ($Na_2WO_4 \cdot H_2O$, 99.5%) and nitric acid (≤ 20%) were obtained from Sinopharm Chem. CO_2 and Ar (99.999%) were provided by Nanjing Special Gas Company. Unless otherwise specified, all the materials were used as received without further purification.

Synthesis of $WO_3 \cdot H_2O$ nanosheets

Typically, 10 mg sodium tungstate dihydrate were dissolved in 10 mL deionized water with vigorous stirring at room temperature for 30 minutes, followed by rapidly adding 1 mL nitric acid and kept for another 22 h. The color of solution changed from milky to pale yellow. The resulted suspension was washed with absolute ethyl alcohol several times and dried in oven at 80 °C for 12 h. Afterwards, the obtained $WO_3 \cdot H_2O$ powder was finely ground for further use.

Synthesis of WO_{3-x}

The WO_{3-x} catalysts were obtained by placing the multilayer $WO_3 \cdot H_2O$ precursor (50 mg) in the tube furnace and calcined at 450 °C for 40 and 60 min under a hydrogen flow (H_2/Ar, v/v = 20%), or calcined at 700 °C for 5 s in air, denoted as H-40, H-60, and A-5, respectively.

Materials characterizations

Transmission electron microscope (TEM) was utilized to investigate the morphology of the photocatalysts. High-resolution transmission electron microscope (HRTEM) images of H-40 was obtained using a transmission electron microscope (JEM-ARM200F NEOARM, Japan) operated at an accelerating voltage of 200 kV. High-resolution transmission electron microscope (HRTEM) images of other samples were obtained using an emission electron microscope (JEOL JEM-F200, Japan) operated at an accelerating voltage of 200 kV. The TEM samples were prepared by dropping the solution onto a molybdenum grid with ultrathin carbon supporting film and dried in air. Electron paramagnetic resonance (EPR) spectrogram were recorded using an EPR spectroscopy (Bruker EMXnano, Germany) at 100 K. X-ray photoelectron spectroscopy (XPS) measurements of samples were carried out using a X-ray photoelectron spectrometer with Al Kα as the X-ray source, and all binding energy of samples were corrected by referencing the C 1s peak to 284.8 eV. The crystal structures of the samples were analyzed by using an X-ray powder diffractometer (SmatrLab9kW, Japan) equipped with Cu Kα radiation (λ = 0.15418 nm). The Fourier transform infrared (FT-IR) spectrum was recorded on a FT-IR spectrometer (Thermofisher Nicolet iS 50, American). The Raman spectra were obtained on a Raman spectrometer (Horiba Xplora Plus, France) spectrometer with a 532 nm laser. The specific surface area was obtained by the Brunauer-Emmett-Teller (BET) method and measured by using a Micromeritics ASAP 2020 at 77 K with N_2 physical adsorption. The photoluminescence spectra were obtained with an exciting wavelength of 320 nm, and samples decay curves were recorded on a FLUORMAX-4P spectrophotometer (Horiba Jobin Yvon, France). The UV-vis absorption was recorded using a UV-3600 UV-vis spectrophotometer.

Photocatalytic study

The photocatalytic CO_2 reduction with H_2O was conducted in Labsolar-6A system (Beijing Perfectlight Technology Co. Ltd). A home-made and airtight quartz container was used as the reactor. 8.5 mg photocatalyst was dispersed in 0.15 mL ethanol to form uniform ink and the photocatalyst ink was spread on the round quartz slide and dried overnight. Then the quartz slide with the photocatalyst was flatly placed in the middle of the reactor. Before the photocatalytic test, the reactor was filled with the ultrapure CO_2 by aerating CO_2 for 0.5 h, and 20 mL water was added in the bottom of reactor as the proton source. The 300 W Xenon light was used as the light source. The reaction system temperature was controlled at 278 K through recycle cooling water system. The gas products were quantified on-line by the gas chromatograph (Agilent GC 8860) using argon as the carrier gas. Meanwhile, the liquid products were quantified by nuclear magnetism resonances (JNM-ECZ600R).

Quantum efficiency calculations

In the following, we describe the QE determination at λ_0 = 334 nm for WO_3 catalysts. The catalyst was irradiated by a 300 W Xe lamp. The average intensity of irradiation was determined to be 0.707 mW cm^{-2} by an PL-MV2000 spectroradiometer (Perfectlight) and the irradiation area was 12.56 cm^2. The number of incident photons (N) is 5.37×10^{19} as calculated by following equation.[1] The amount of CH_4 and CH_3OH molecules generated in 1 h was 0.75 μmol g^{-1} and 4.02 μmol g^{-1} (**Fig. 3b**). The quantum efficiency is outlined below:

$$N = \frac{E\lambda}{hc} = \frac{7.07 \times 10^{-4} \times 12.56 \times 3600 \times 334}{6.626 \times 10^{-34} \times 3 \times 10^{17}} = 5.37 \times 10^{19}$$

$$QE = \frac{\text{the number of reacted electrons}}{\text{the number of incident photons}} \times 100\%$$

$$= \frac{\left(8 \times 0.75 \times 10^{-6} + 6 \times 4.02 \times 10^{-6}\right) \times 6.02 \times 10^{23} \times 8 \times 10^{-3}}{5.37 \times 10^{19}} \times 100\% = 0.27\%$$

Electrochemical study

The photoelectrochemical test of the catalysts were evaluated in a typical three-electrode system using the electrochemistry workstation (CHI 760E).[2] The catalyst ink was spread on the fluorine-doped tin oxide (FTO) glass as working electrodes. For a typical procedure, 10 mg catalyst and 100 μL Nafion 117 solution were dispersed in a mixed solution of 0.2 mL of ethanol and 0.7 mL ultrapure water to form the homogeneous catalyst ink. Then, 200 μL catalyst ink was spread on the FTO glass and dried at room temperature naturally. The Ag/AgCl electrode and Pt foil were used as the reference electrode and counter electrode, respectively. The photocurrent response tests were conducted under a 300 W Xenon light (PLs-SXE300+, Perfect light, China) illumination. Chronoamperometry tests were conducted at 0.5 V vs Ag/AgCl. The Mott-Schottky plots were tested at the frequency of 1000 Hz in 0.5 M $KHCO_3$ electrolyte.

Electrochemical impedance spectroscopy (EIS) was carried out in Swagelok in the frequency range of 0.01 to 1×10^6 Hz at a scan rate of 0.1 mV s^{-1}.

Carrier density calculations

The carrier density (N_d) can be estimated by the following equations:[3]

$$N_d = \frac{2}{e\varepsilon\varepsilon_0}\left[\frac{d\left(\frac{1}{C^2}\right)}{d(E)}\right]^{-1}$$

where C is the capacitance of the space charge layer, N_d is the number of donors, e (1.602×10^{-19} C) is the electron charge, ε (20 for WO_3) is the dielectric constant, and ε_0 (8.85×10^{-14} F cm^{-1}) is the vacuum permittivity, and E is the applied potential.The positive slopes indicate the n-type nature of all WO_3 samples.

In-situ FT-IR study

In-situ FT-IR was obtained using a Thermofisher Nicolet iS 50. The sample was placed in the reaction cell and pressed to keep the surface flat, then sealed and purged with Ar to remove surface impurities. After the sample reached adsorption equilibrium under CO_2 atmosphere, the Xenon lamp was then started to illuminate the sample and recorded after a certain time interval.[4]

Calculation details

The calculation was carried out by the spin-polarized periodic density functional theory implemented in the Vienna *ab initio* simulation package (VASP).[5] The interaction between the core and valence electrons was described using the frozen-core projector augmented wave (PAW) approach.[6] The generalized gradient approximation (GGA) with the Perdew-Burke-Ernzerhof (PBE)[7] functional was used to describe the exchange-correlation energy. The cutoff energy was set to 500 eV. For considering and correcting the long-range Van der Waals interactions, the DFT-D3 method with Becke-Jonson damping was employed in this work.[8] The calculated lattice parameters of bulky WO_3 are a = 7.42 Å, b = 7.57 Å and c = 7.75 Å, in agreement with the experimental values, a = 7.30 Å, b = 7.54 Å and c = 7.69 Å. Herein, we used a $(\sqrt{2}\times\sqrt{2})$-R45° supercell[9] with a thickness of 7 atomic layers containing 96 ($W_{24}O_{72}$) atoms to mimic the perfect surface model. The vacuum slab thickness was set up to 15 Å to eliminate layer to layer interactions. During the optimization, the bottom three layers atoms were fixed, while the top four layers atoms along with those adsorbed species were fully relaxed. The geometry optimization stops until forces on atoms smaller than 0.02 eV/Å. The total energy converge was set to be less than 10^{-5} eV. For the first Brilliouin zone a 3×3×1 k-point grid was sampled following the Gamma-centered-grid scheme.[10] The Bader type charge was computed to analyze the charge transformation properties of the system.

The free energy diagrams for CO_2 reduction to CH_3OH were calculated with reference to the computational hydrogen electrode method (CHE) proposed by Nørskov et al.[11] The chemical potential of a proton-electron pair ($\mu[H^{+}+e^{-}]$) at U = 0 V equals to half of hydrogen ($0.5\mu[H_2]$) at 1 bar of H_2 and 298 K. Consequently, the free energy of each species can be obtained from the following equation.

$$G = E + \mathrm{ZPE} - TS$$

where E is the electronic energy of these species from the DFT calculation, ZPE is the zero-point energy, T is the temperature and S the entropy, respectively.

As stated before, the perfect $WO_3(001)$ surface (denoted as WO_3 in the main text) was utilized to mimic the pristine metal oxide surface. Apart from the perfect model, 4 atop-like O atoms were removed within the perfect model to simulate the as-synthesized pit-decorated catalyst (denoted as WO_{3-x} in the main text).

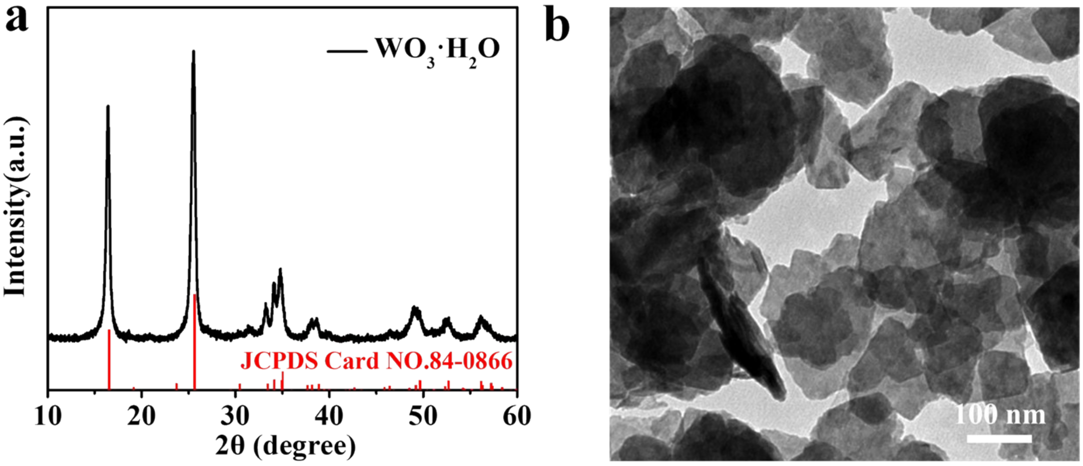

Fig. S1. a) XRD pattern and b) TEM image of the $WO_3·H_2O$ nanosheets.

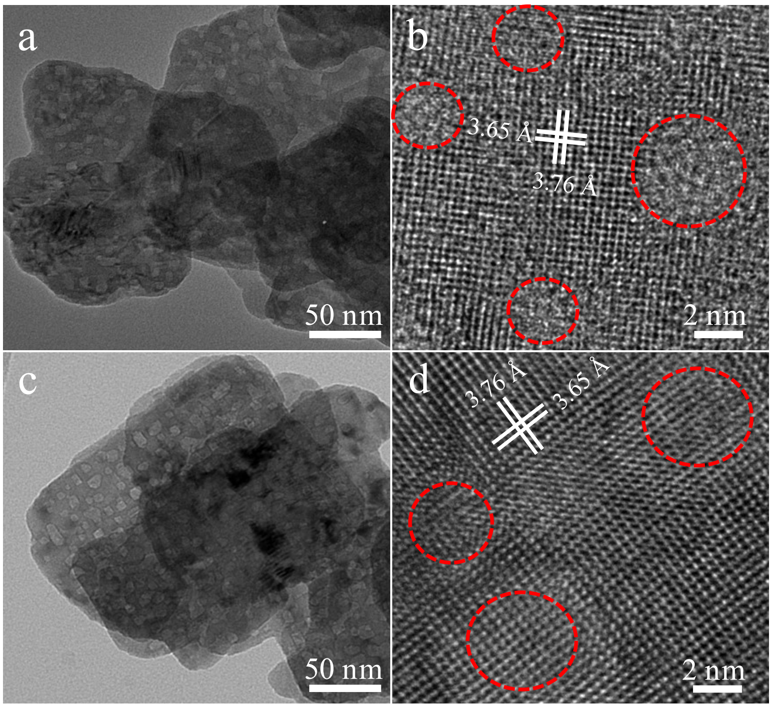

Fig. S2. TEM and HRTEM images of a) and b) A-5; c) and d) H-60, respectively.

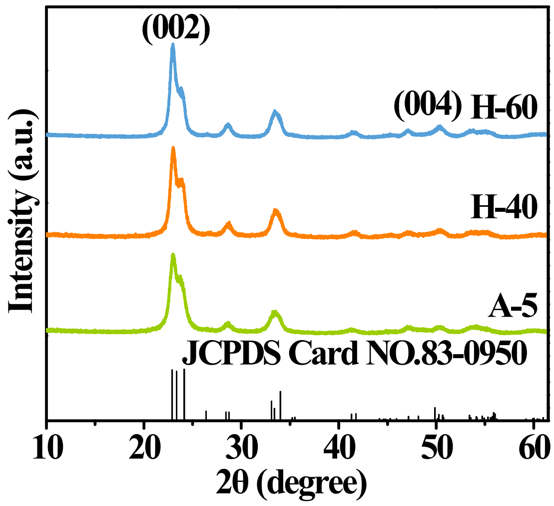

Fig. S3. XRD patterns of A-5, H-40, and H-60, respectively.

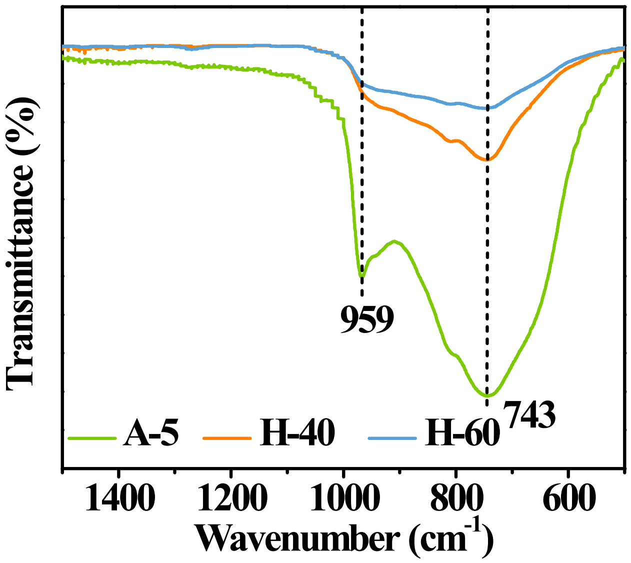

Fig. S4. FT-IR spectra of different WO_3 nanosheets.

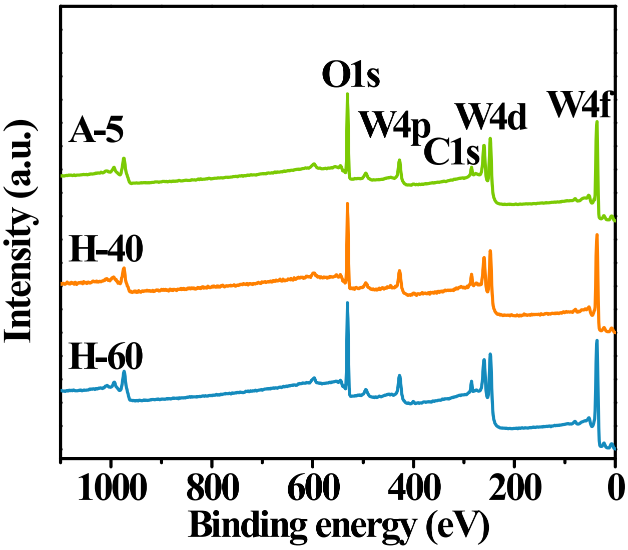

Fig. S5. XPS survey spectra of A-5, H-40, and H-60, respectively.

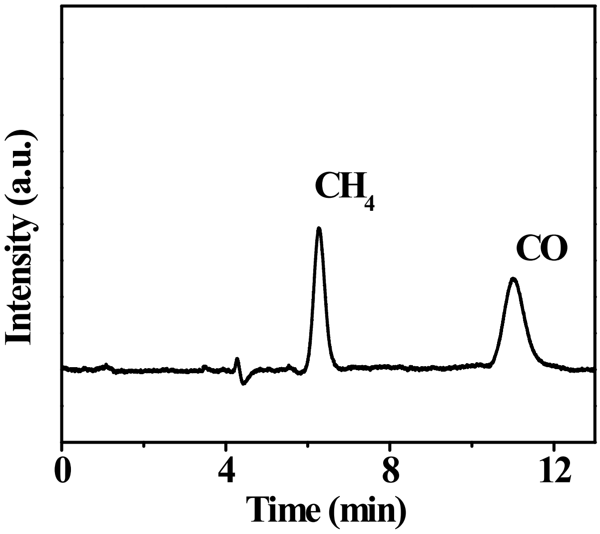

Fig. S6. GC spectra for gaseous products of A-5.

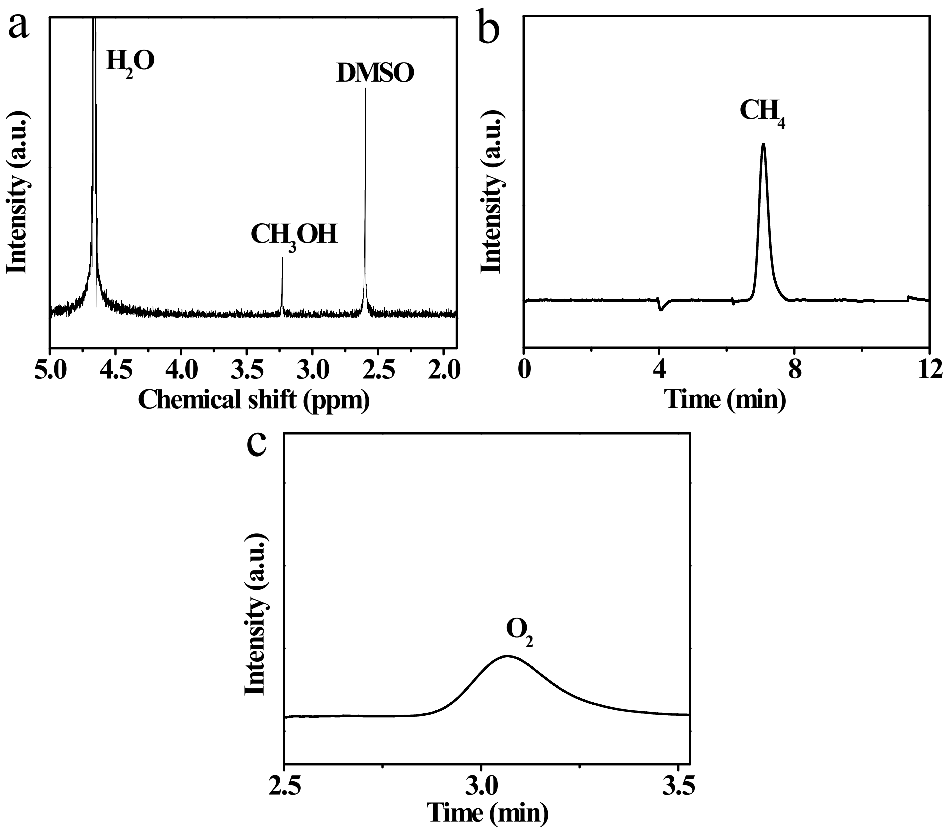

Fig. S7. a) The liquid and b-c) gaseous products of H-40.

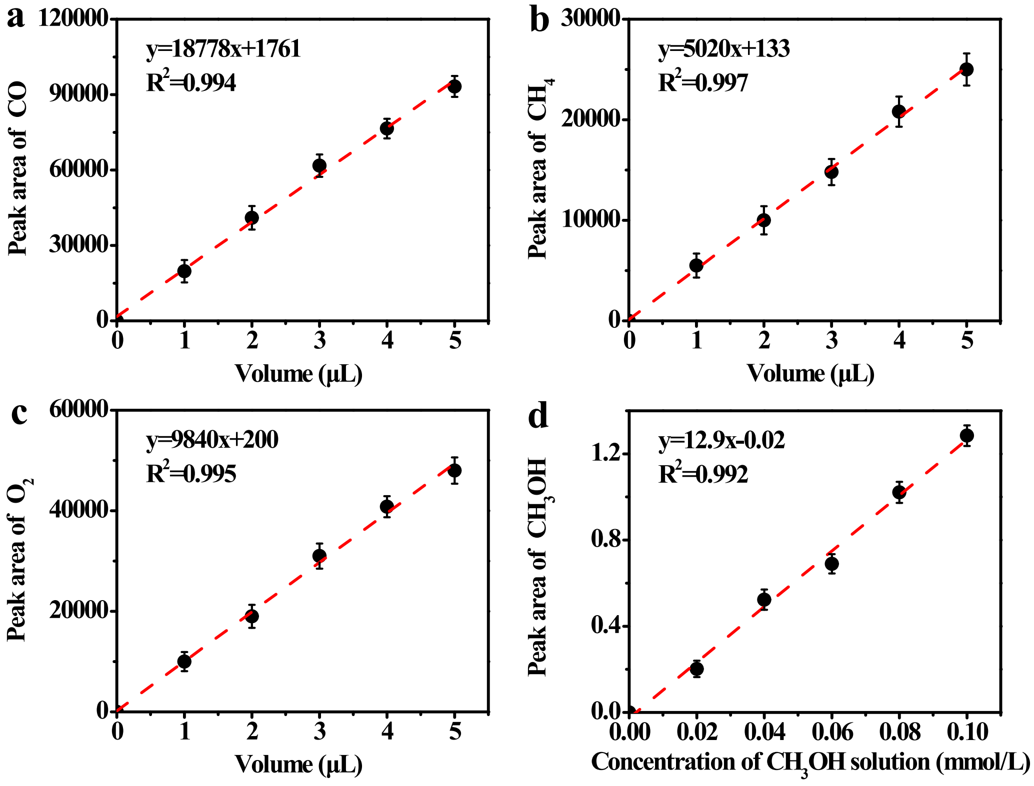

Fig. S8. The standard curve for the detection of CO a), H_2 b), O_2 c) and CH_3OH d) products.

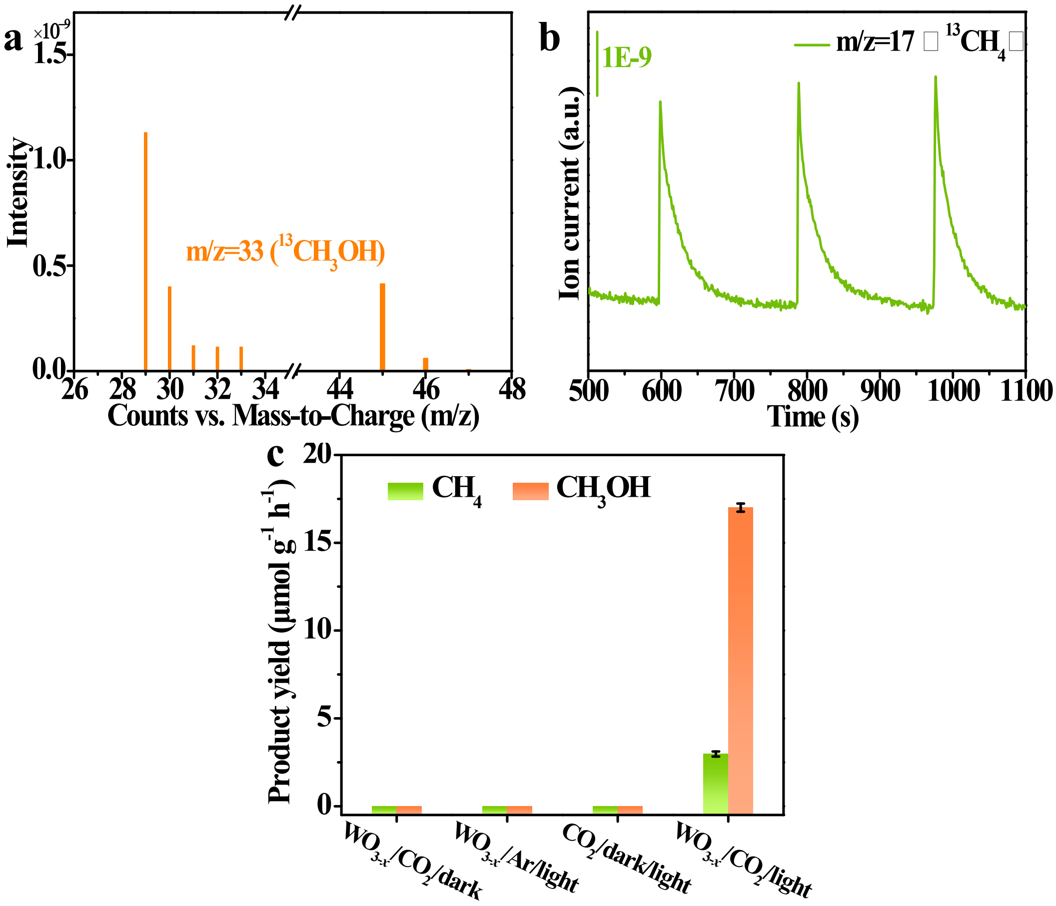

Fig. S9. Mass spectra of ^{13}C-labled CH_4 a) and CH_3OH b) products over H-40. c) Products of photocatalytic CO_2 reduction for H-40 under different work conditions.

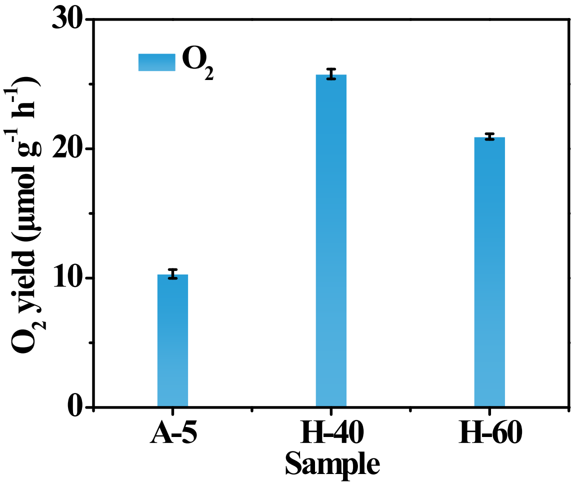

Fig. S10. Yields of O_2 on different WO_3 nanosheets.

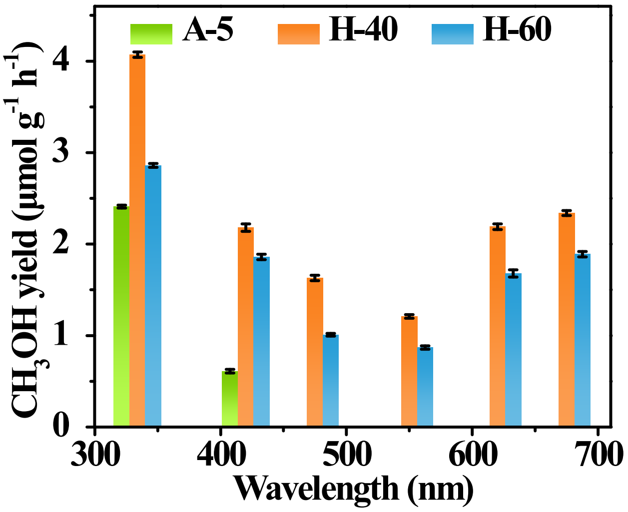

Fig. S11. The CH_3OH yields of A-5, H-40, and H-60 at different wavelengths, respectively.

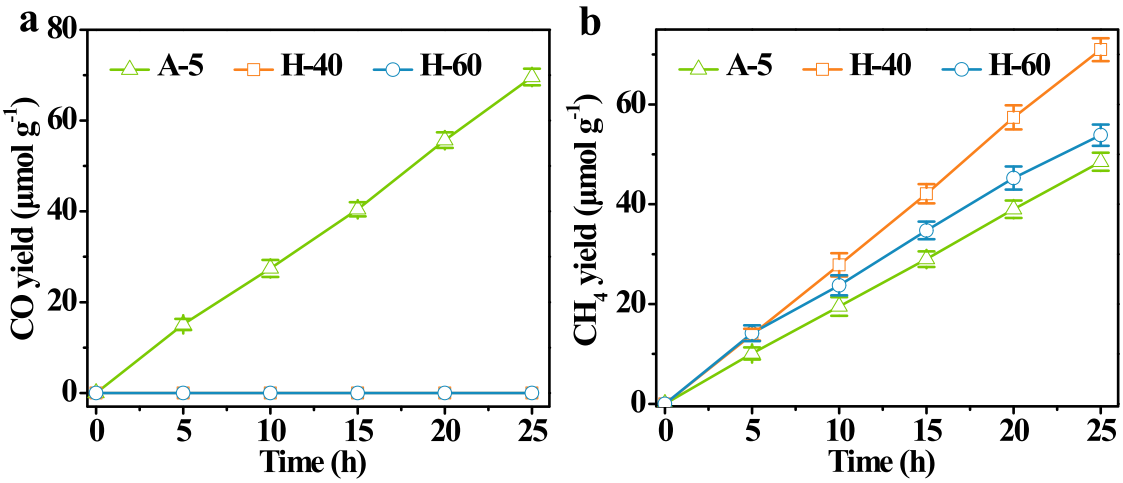

Fig. S12. Time-dependent photocatalytic a) CO and b) CH_4 evolution curves of A-5, H-40, and H-60 at 5 °C.

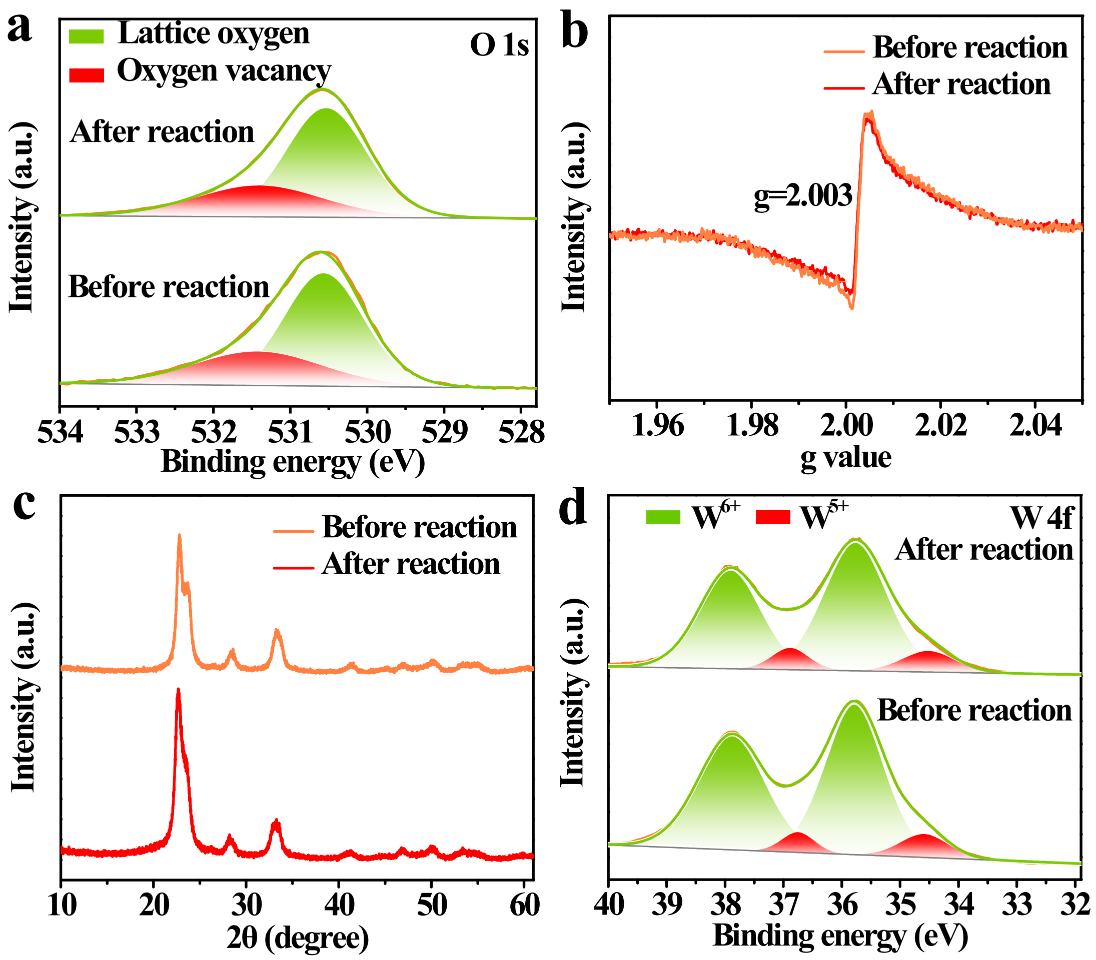

Fig. S13. a) O 1s XPS spectra, b) EPR spectra, c) XRD patterns, d) W 4f XPS spectra of H-40 before and after photocatalysis.

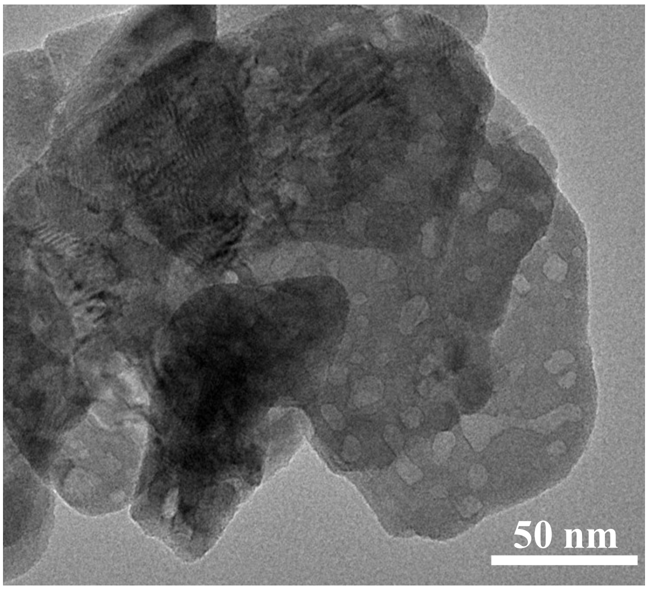

Fig. S14. TEM image of H-40 after photocatalysis.

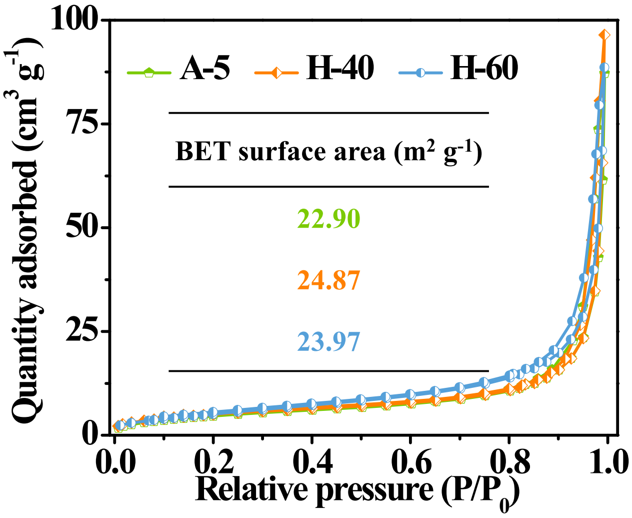

Fig. S15. Nitrogen adsorption-desorption isotherms of different WO_3 nanosheets.

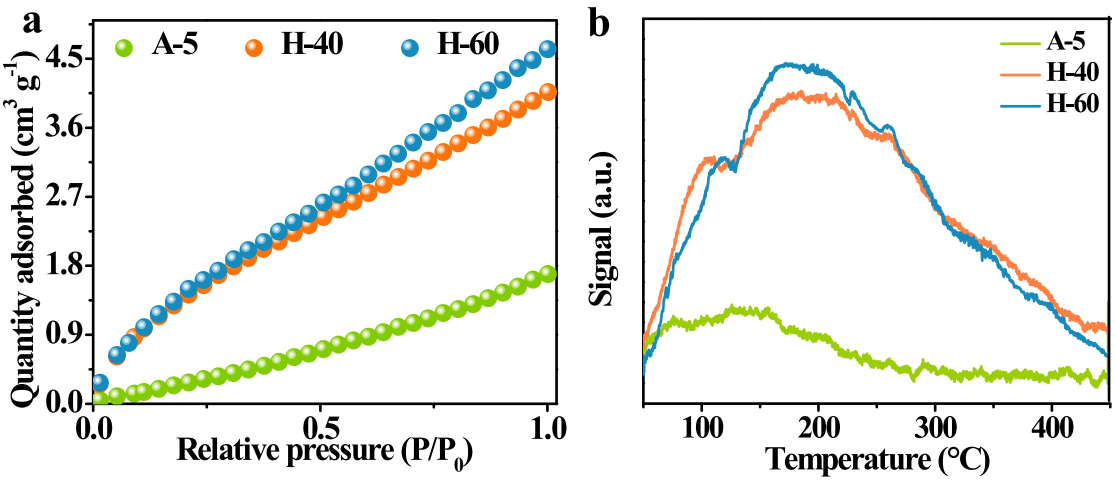

Fig. S16. a) CO_2 adsorption isotherms and b) CO_2-TPD spectra of A-5, H-40, and H-60, respectively.

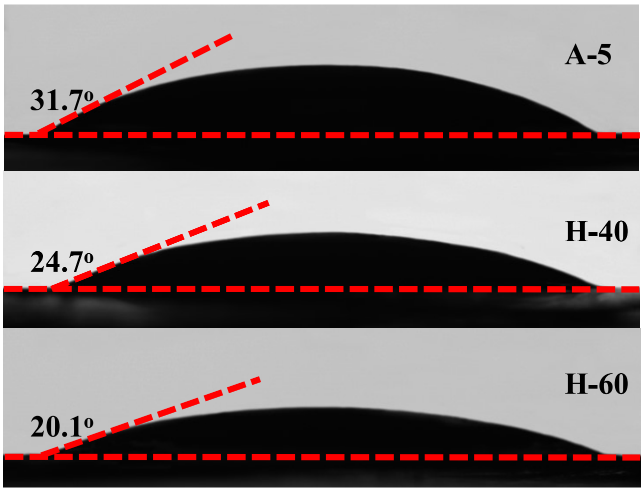

Fig. S17. Water contact angle measurements of A-5, H-40, and H-60, respectively.

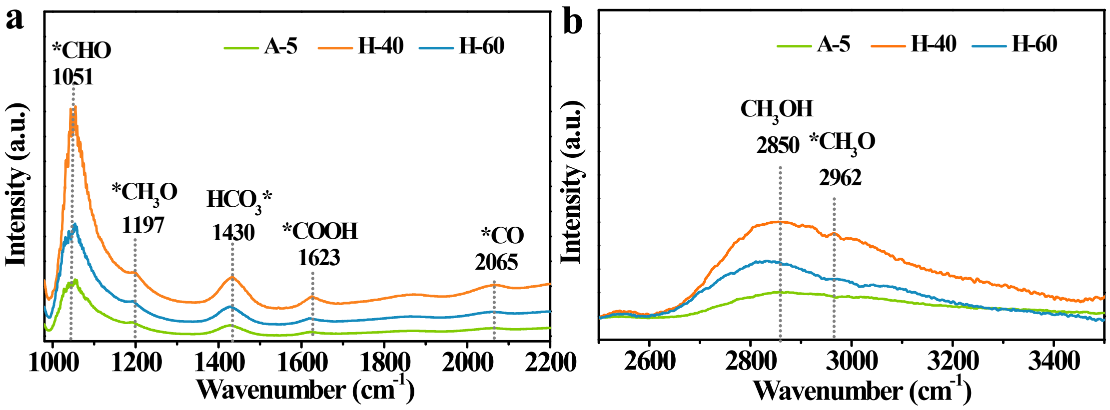

Fig. S18. *In-situ* FT-IR spectra of A-5, H-40, and H-60 under 25 min illumination.

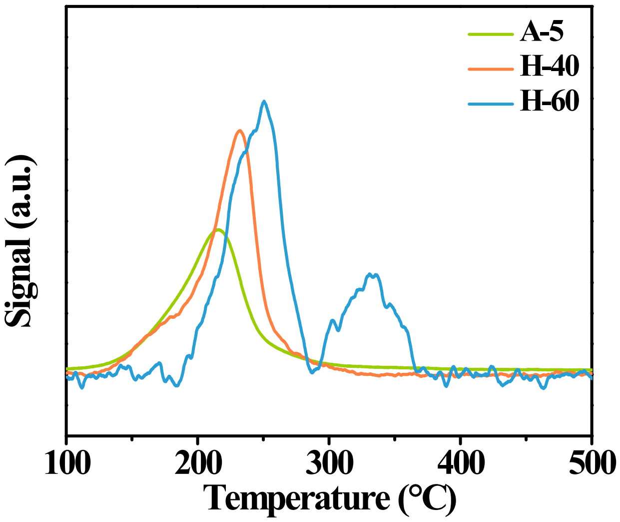

Fig. S19. CO-TPD spectra of A-5, H-40, and H-60, respectively.

Table S1. The peak area ratio of different W valence (W^{6+}, W^{5+}), lattice oxygen and oxygen vacancy of different samples.

Materials	W^{6+} (%)	W^{5+} (%)	Lattice oxygen (%)	Oxygen vacancy (%)
A-5	98.11	1.89	87.94	12.06
H-40	90.82	9.14	67.05	32.95
H-60	85.76	14.24	60.42	39.58

Table S2. Characterizations of H-40 after photocatalysis, the peak area ratio of different W valence (W^{6+}, W^{5+}), lattice oxygen and oxygen vacancy.

Materials	W^{6+} (%)	W^{5+} (%)	Lattice oxygen (%)	Oxygen vacancy (%)
Before reaction	90.82	9.14	67.05	32.95
After reaction	90.91	9.03	67.92	32.08

Table S3. Time-resolved transient PL decay of A-5, H-40, and H-60.

Materials	τ_1 (ns)	τ_2 (ns)	τ_3(ns)
A-5	0.55	3.49	18.0
H-40	0.92	4.11	21.0
H-60	0.76	3.97	20.2

Table S4. Photoelectrochemical property of various photoanodes.

Materials	R_{CT} [Ω]	N_d [10^{19} cm^{-3}]	The top of valence band [eV]
A-5	52600	0.428	2.61
H-40	3800	3.319	1.91
H-60	2700	2.21	1.65

Reference

1 J. Liu, Y. Liu, N. Liu, Y. Han, X. Zhang, H. Huang, Y. Lifshitz, S. Lee, J. Zhong and Z. Kang, *Science*, 2015, **347**, 17-21.

2 Z. Wang, L. Zhang, T. U. Schulli, Y. Bai, S. A. Monny, A. Du and L. Wang, *Angew. Chem. Int. Ed.*, 2019, **58**, 1-7.

3 Y. Zhao, Y. Zhao, R. Shi, B. Wang, G. I. N. Waterhouse, L. Z. Wu, C. H. Tung and T. Zhang, *Adv. Mater.*, 2019, **31**, 1806482.

4 a) J. Wu, X. Li, W. Shi, P. Ling, Y. Sun, X. Jiao, S. Gao, L. Liang, J. Xu, W. Yan, C. Wang and Y. Xie, *Angew. Chem. Int. Ed.*, *2018*, **130**, 8855-8861; b) X. Li, Y. Sun, J. Xu, Y. Shao, J. Wu, X. Xu, Y. Pan, H. Ju, J. Zhu and Y. Xie, *Nat. Energy*, 2019, **4**, 690.

5 G. Kresse and J. Furthmuller, *Phys. Rev. B*, 1996, **54**, 1169-1172.

6 a) P. E. Blochl, *Phys. Rev. B* 1994, **59** ,17993; b) G. Kresse and D. Joubert, *Phys. Rev.*, 1999, **59**, 1758-1762.

7 J. Perdew, K. Burke and M. Ernzerhof, *Phys. Rev. Lettb.*, 1996, **77**, 3865-3870.

8 S. Grimme, J. Antony, S. Ehrlich and H. Krieg, *J. Chem. Phys.*, 2010, **132**, 154104.

9 a) F. Wang, C. Valentin and G. Pacchioni, *J. Phys. Chem. C*, 2012, **116**, 10672-10679; b). E. Albanese, C. Valentin and G. Pacchioni, *ACS Appl. Mater. Interfaces*, 2017, **9**, 23212-23221.

10 H. J. Monkhorst and J. D. Pack, *Phys. Rev. B*, 1976, **13**, 5188-5192.

11 J. Nørskov, J. Rossmeisl, A. Logadottir, L. Lindqvist, J. Kitchin, T. Bligaard and H. Jonsson, *J. Phys. Chem. B*, 2004, **108**, 17886-17891.